TECHNISCHE UNIVERSITÄT WIEN
Vienna University of Technology

Diplomarbeit

Implementation of a line-scanning laser ophthalmoscope into an adaptive optics system

Ausgeführt am
Institut für Angewandte Physik
der Technischen Universität Wien

unter der Anleitung von
Ao.Univ.Prof. Dipl.-Ing. Dr.techn. Martin Gröschl

in Zusammenarbeit mit
Assoc. Prof. Priv.-Doz. Dipl.-Ing. Dr. Michael Pircher

Zentrum für Medizinische Physik und Biomedizinische Technik
der Medizinischen Universität Wien

durch
Paul Vetschera BSc
Gatterburggasse 11/12
1190 Wien

February 2014

Abstract

The combination of adaptive optics with scanning laser ophthalmoscopy (AO-SLO) is a promising high-resolution, optical imaging technique that enables to study non-invasively human photoreceptors in vivo. To date these complex instruments are only available for a few scientific groups worldwide. Nevertheless this technology already provided valuable insights for ophthalmologists and is expected to be translated into clinical routine in the near future. One drawback of such systems is the limited field of view. Thus, secondary overview scans of the retina are required in order to better locate the scanning area on the human eye fundus. Within this master thesis, a separate line-scanning laser ophthalmoscope (LSLO) was designed and implemented into an existing AO-SLO system. The first part of this thesis gives an introduction to retinal imaging methods and their combination with AO. Subsequently, the thesis explains the design, implementation and alignment of the LSLO. The final part deals with the characterization of the LSLO performance and shows first imaging results obtained from healthy volunteers.

Kurzfassung

Die Kombination eines Laser Abtast-Ophthalmoskops mit Adaptiver Optik (LAO-AO) ist ein vielversprechendes, hochauflösendes Bildgebendes Verfahren, mit dessen Hilfe man menschliche Photorezeptoren nichtinvasiv und in vivo studieren kann. Derzeit stehen diese sehr komplexen Geräte nur einigen, wenigen wissenschaftlichen Gruppen weltweit zur Verfügung. Nichtsdestotrotz ermöglicht diese Technik wertvolle Einsichten für Ophthalmologen und es ist zu erwarten, dass diese Technik auch bald in der klinischen Praxis angewendet werden kann. Ein Nachteil dieser Technik ist der sehr kleine Bildbereich der aufgenommen werden kann. Deshalb werden sekundäre Übersichtsbilder benötigt, um den abgebildeten Bereich des Augenhintergrundes besser lokalisieren zu können. Im Rahmen dieser Diplomarbeit wurde ein zusätzliches Linien-Abtast- Laser Ophthalmoskop entwickelt und in ein bereits existierendes LAO-AO Gerät eingebaut. Der erste Teil der Arbeit beschreibt bildgebende Verfahren und deren Kombination mit Adaptiver Optik. Danach werden in dieser Arbeit das Design, die Implementierung und die Justage des Gerätes erläutert. Der abschließende Teil charakterisiert die Eigenschaften des Linien-Abtast-Laser Ophthalmoskops und zeigt erste Bildergebnisse von gesunden Probanden.

Acknowledgements

I gratefully wish to thank my supervisor Prof. Michael Pircher from the Medical University of Vienna, for giving me this splendid opportunity to work at the Center of Medical Physics and Biomedical Engineering and for supporting me throughout the whole thesis period. Moreover, I want to thank my supervisor Prof. Martin Gröschl from the Institute of Applied Physics at the Vienna University of Technology, who established the contact to the Medical University of Vienna and gave me the opportunity to work there.

Especially, I want to thank my colleague DI Franz Felberer, who was working with me in the lab and always supported me if I had any question. Thanks to my group colleague Julia Kroisamer, who provided important reference images to me. Moreover, I want to thank all the colleagues at the Center for Medical Physics and Biomedical Engineering. They gave me a friendly welcome, there was a great working atmosphere and many colleagues were also very curious about my work. Special thanks belong to the mechanical workshop member who supplied me with important components. Furthermore, I particularly want to thank my parents Ursula and Rudolf Vetschera for proof reading and advising.

Contents

Table 1: List of abbreviations

AMD	Age-related macular degeneration
ASE	Amplified spontaneous emission
AO	Adaptive optics
AO-SLO	Adaptive optics scanning laser ophthalmoscope
CCD	Charged-coupled device
CRB	Corneal reflections blocker
cSLO	confocal Scanning laser ophthalmoscope
DM	Deformable mirror
DiM	Dichroic mirror
DOF	Depth of field
DR	Diabetic retinopathy
EC	Entrance collimator
EL	Eye lens
FOV	Field of view
FPA	Focal plane array
FPGA	Field-programmable gate array
FPS	Frames per second
FWC	Full well capacity
GS	Galvo scanner
LSLO	Line-scanning laser ophthalmoscope
LS	Light source
M	Mirror
MPE	Maximum power emission
NA	Numerical aperture
OCT	Optical coherence tomography
P	Pellicle
PMT	Photomultiplier tube
ONH	Optic nerve head
PBS	Polarizing beam splitter
PQS	Peak quantum efficiency
ROI	Region of interest
SH	Shack-Hartmann
SLO	Scanning laser ophthalmoscope
SNR	Signal-to-noise ratio

Chapter 1

Introduction and motivation

The human eye has always been among the most fascinating sensory organs in human beings. Without vision, every aspect of life will be much harder. Vision defects usually strongly disturb the subject's daily routines and lead to a loss of quality of life. The most frequent vision defects are caused by disorders of the anterior segment (e.g. lens) such as cataract. However, in the industrialized world disorders of the posterior eye segment (retinal disorders) such as age-related macular degeneration (AMD) and diabetic retinopathy (DR) belong to the most frequent reasons for degradation of vision [1]. Retinal imaging devices such as ophthalmoscopes have nowadays become indispensable for diagnosis of these diseases.

In vivo examinations of the posterior eye segment have remained challenging for centuries. Modern ophthalmology therefore started not earlier than in 1851, with the invention of the ophthalmoscope by Helmholtz. The instrument enabled first insights in the posterior segment of the living eye [2]. Figure 1.1 illustrates the basic principle of an ophthalmoscope.

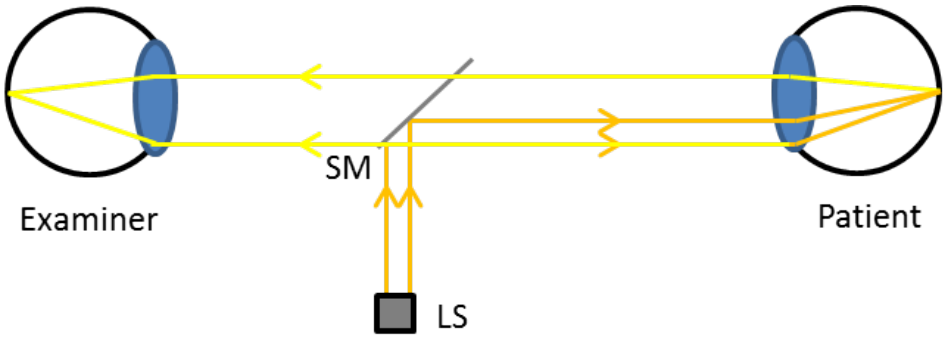

Figure 1.1: Principle of Helmholtz' opthalmoscope, adapted from F. Grehn [2]. SM: Semi-transparent mirror, LS: Light source

Since then, ophthalmoscopes have been developed at an enormous rate, finally leading to modern scanning laser ophthalmoscopes (SLO) and instruments capable to provide high-resolution images of the eye fundus including the visualization of single photoreceptors (cones and rods) [3, 4].

Meanwhile, the anatomy of the human eye is well known. The diameter of the eyeball of an adult is approximately 24mm. The eyeball consists of the cornea, sclera, lens, vitreous, iris, choroid and retina. Figure 1.2 schematically depicts major parts of the human eye. The sclera and the transparent cornea wrap up the eyeball, the iris serves as aperture and regulates the light intensity incident on the retina. The cornea and the eye lens focus incident light beams on the photoreceptor cells that are part of the retina. These convert the incoming light into electrical signals which are preprocessed before they are transmitted via the optic nerves to the optic nerve head (ONH). The electric signals exit the eye through the ONH (location of the blind spot) and are transmitted to the visual cortex of the brain. In the healthy eye, the location with the sharpest vision (i.e. the location of fixation) is the fovea. The fovea contains the highest packing density of cones (which enable color vision) and does not contain rods (which are responsible for bright/dark vision) [2]. Cones can be divided into three groups that are sensitive to short, medium and long wavelengths respectively (roughly red, green, blue)[5]. Photoreceptors are connected to bipolar cells, which are connected to ganglion cells. Together, all these cells represent the three neurons of the retina [2]. The choroid is responsible for the blood supply of the outer retina [6].Figure 1.3 illustrates the retinal structure schematically [6]. More information can be found in [2] and [6].

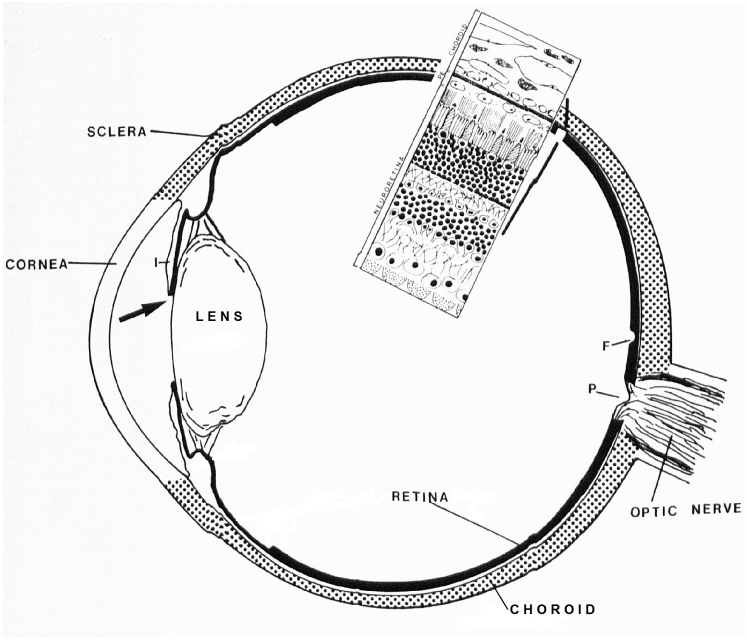

Figure 1.2: Scheme of an adult eye. I: Iris, P: Papilla nervi optici - optic nerve, F: Fovea. Source: W. Krebs, I. Krebs [6]

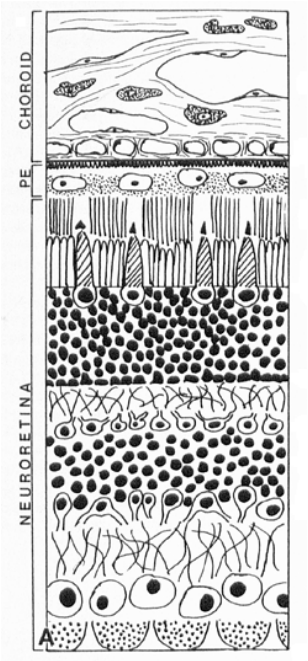

Figure 1.3: Scheme of the human retina, adapted from W. Krebs [6]. PE: Pigment epithelium. The neuroretina consists of nine main layers. Source: W. Krebs, I. Krebs [6]

In order to be able to detect retinal diseases, a certain resolution is required. Fundus cameras, optical coherence tomography and SLOs are clinically used

to generate images of the retina. However, imperfections of the eye optics limit the lateral resolution of all these imaging devices and prevents imaging on a cellular level in most subjects. This is where adaptive optics (AO) comes into play. AO is a technique known from astronomy. It measures the wavefront exiting the eye (which is distorted by imperfections of the eye optics) and corrects it using a correcting device (e.g. deformable mirror (DM)) [4, 7]. With this technology very sharp images of the retina were obtained [5] and even rod cells could be resolved in vivo [8]). However, in AO systems the field of view (FOV) is limited, because aberrations vary within larger field of views and thus AO-correction can only be achieved within a small FOV where aberrations can be assumed to be constant. Due to the small FOV provided by AO-SLO system-scans, the determination of the exact location is in general difficult and may be erroneous. Therefore it is advantageous to have a second overview image that is ideally recorded simultaneously to locate the AO FOV on the retina. A special form of the SLO is the Line-Scanning Laser Ophthalmoscope (LSLO). The LSLO has several interesting characteristics that make it a good candidate for a supplementing system to the AO-SLO.

The aim of this master thesis is to build, characterize and implement a LSLO into an existing AO-SLO system at the Medical University of Vienna in order to provide overview images of the retina during the recording of AO-SLO images. The LSLO is based on a concept for LSLO introduced by Hammer et al [9]. The new LSLO constructed within this thesis uses a broadband infrared light source with a central wavelength of 1050nm so that it can easily be combined with the existing AO-SLO (central wavelength at 840nm) using a dichroic mirror. The optical path is lens based, the transformation of the gaussian beam profile exiting the fiber to a line profile is performed by a cylindrical lens. The backscattered light from the retina is detected by a special line-array charged couple-device (CCD) camera that is sensitive in the 1050nm wavelength range.

The first part of this thesis gives an introduction to retinal imaging methods that can be combined with AO. Subsequently, the thesis explains the design, implementation and alignment of the LSLO. The final part characterizes the LSLO performance and shows first imaging results.

Chapter 2

Retinal imaging methods

This section shortly describes basic retinal imaging techniques such as fundus cameras, scanning laser ophthalmoscopes and optical coherence tomography. It includes historic developments and subsequently explains the principles. Finally the combination of AO with these techniques is described. More detailed information can be found in literature (e.g. [3, 4, 7, 10]-[12]).

2.1 Fundus cameras

The classical retinal imaging instrument is the fundus camera which enables to take color photographs of the human eye fundus. Fundus cameras are routinely used in clinics and provide a two dimensional view of the posterior segment of the eye. Fundus cameras generate wide-field retinal images up to 60° field of view [10]. The lateral resolution within the images is limited by the optics of the eye [4].

The typical transverse resolution of these images is about $\sim 50\mu m$. Image magnification is already achieved by using the optics of the imaged eye. The main drawback of fundus cameras is the lack of depth sectioning. As mentioned above, the retina consists of a variety of layers which cannot be resolved using this technique.

2.2 Scanning laser ophthalmoscopes and confocal scanning laser ophthalmoscopes

The scanning laser ophthalmoscope (SLO) is a retinal imaging device that illuminates the retina with a flying laser beam spot and detects the backscattered

light [3]. Firstly published in 1981 [3], the technique uses two scanning mirrors and appropriate electronics to move the flying spot in two directions [3]. The first SLO versions used photomultiplier tubes (PMTs) and TV-electronics for detection, whereas nowadays modern SLOs use PMTs or avalanche photo diodes (APD) in combination with a computer based data acquisition [3, 4]. One of the SLO's main advantages in comparison to fundus cameras is the higher contrast [10]. This yields better results for retinal monitoring for patients e.g. suffering from cataract [10].

An improved version of the SLO is the confocal scanning laser ophthalsmoscope (cSLO). As a technique from the late eighties, its main idea is based on detecting mainly the backscattered light from the focal point [11]. This focal point is imaged to a conjugate plane before the detector where a pinhole is placed. The purpose of the pinhole is to reject out of focus light. This approach yields higher contrast images in comparison with non-confocal imaging systems and additionally a depth sectioning capability is achieved [11].

2.3 Line-scanning laser ophthalmoscopes

One of the first line-scanning laser ophthalmoscope was developed by D.X. Hammer et al. in 2006 [9]. In contrast to standard SLOs where a laser spot is moved over the retina, a laser line is projected on the retina. The backscattered light is then detected with a line-scan camera. Consequently, the number of scanners is reduced, only one galvanometer scanner (GS) for the orthogonal direction (y-direction) is needed. The LSLO fills the niche between expensive high resolution retinal imaging devices and low-cost, low-resolution devices [9]. Furthermore, more power can be applied to the eye when using the LSLO. This is due to the distribution of the light power on the retina in a line. On the downside, confocality as obtained with the cSLO is only achieved in one direction (orthogonal to the line).

2.4 Optical coherence tomography

Optical coherence tomography enables high-resolution, cross-sectional imaging of biological tissue in vivo. It is based on low-coherence interferometry. The backscattered light of the biological sample and light that is reflected by a reference mirror is brought to interference and the resulting interference

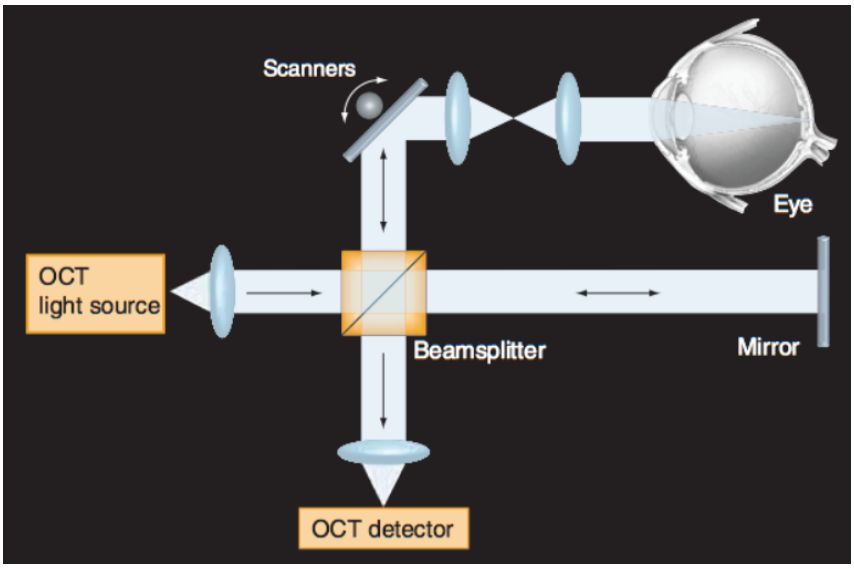

Figure 2.1: Basic scheme of an OCT set-up. Source: M. Pircher and R.J. Zawadzki [15]

signal is detected [12]. The technique was developed in the early nineties, using so-called Time-domain OCT (TD-OCT) systems. These early systems were rather slow and provided mostly simple cross-sectional images, whereas modern Fourier-Domain OCT (FD-OCT) instruments are fast enough to provide 3D volume scans in vivo [13]. OCT provides better axial resolution than any other optical retinal imaging device, because axial and transversal resolution are decoupled from each other [13]. The axial resolution depends on the spectral bandwidth and the center wavelength of the light source, while the transversal resolution depends on the numerical aperture (NA) and the central wavelength of the imaging optics [13]. OCT has nowadays found wide-spread applications not only in ophthalmology, but also in other medical areas such as dermatology, gastroenterology or dentistry, and non-medical applications such as nondestructive testing of paints. [14] Figure 2.1 shows a basic OCT set-up schematically.

2.5 Adaptive optics

Adapative optics (AO) has been a catch phrase in the ophthalmic community for more than a decade. Before AO was implemented in retinal imaging methods, transverse resolution of all these techniques has been limited not only by the optics of the eye, but also by higher order aberrations introduced to the imaging light by imperfections of the eye optics. This changed rapidly when

AO was firstly introduced into ophthalmology. The idea of AO is to measure the wavefront of the light exiting the eye and to compensate for aberrations of the wavefront of the imaging light. The technique had a tremendous impact on the resolution limits in retinal imaging. (see [4], [15]). Thanks to AO, the lateral image quality is not limited by the imperfections of the eye anymore [4]. AO in ophthalmology usually consists of three main parts: a wavefront sensor that measures the wavefront of the light backscattered by the retina, a wavefront-correcting device (e.g. a deformable mirror) and a control software [16]. AO systems are usually operated in closed-loop mode, so that the wavefront sensor detects the correction effectiveness immediately [17]. In ophthalmology, wavefront measurements are usually performed by a Shack-Hartmann sensor (SHS) [18]. Aberrations are usually corrected using a deformable mirror [18]. AO itself is no imaging technique, it needs to be combined with one of the imaging techniques mentioned above [16]. The first imaging technique that was combined with AO was fundus photography. AO fundus cameras can be based on a spatially incoherent light source which greatly reduces speckles. However, AO fundus cameras provide no confocal detection scheme [19]. Therefore the axial resolution will be rather low. Thus, it is very interesting to improve the axial resolution by combining AO with SLO or OCT.

2.6 AO combined with SLO and OCT systems

Currently, the sharpest in vivo images of the human retina where taken with AO-SLO instruments [20, 21]. Contrast and resolution of these instruments can be adapted with varying pinholes sizes [19]. In addition, contrast can be improved using dark field illumination schemes [22]. The main applications of the AO-SLO is imaging of very small structures of the retina such as photoreceptors, vasculature or nerve fiber bundles. However, recently functional imaging of the retina gained increasing interest where single cones are stimulated and their responses are observed either electrically or optically [17].

An interesting option for future investigations is the combinations of AO with OCT which provides higher axial resolution and higher sensitivity in comparison to AO-SLO [23]. State of the art OCT technology is the so called Fourier-Domain OCT (FD-OCT). However, FD-OCT is based on recording A-

scans (depth profiles) that are acquired for all depths simultaneously. While this yields a sensitivity advantage for standard OCT imaging, it also suffers from drawbacks when combined with AO. First, the depth of field (DOF) in AO-systems is much smaller than the depth extension of the retina. Therefore only part of the recorded FD-OCT volume will be in focus. Second, the volume acquisition speed is rather slow and artifacts caused by the eye motion are limiting factors.

One drawback of AO-SLO and AO-OCT systems is the limited FOV. The FOV is limited by the isoplanatic angle of the eye because only within this angle the aberrations can be assumed as constant and AO-correction can be applied. As mentioned above the determination of the exact imaging location of AO- instruments can be very difficult. Therefore, it would be beneficial to implement an additional imaging device that is capable to provide overview images of the retina into the AO instruments.

Chapter 3

Experimental setup

This section describes the design of the LSLO and its implementation into the AO-SLO. The first part briefly describes the AO-SLO setup and illustrates associated frame conditions for the LSLO setup. In the second part, the experimental setup, the principle of the method, specific components and their function of the LSLO are presented.

3.1 The Adaptive Optics SLO setup

As stated in the introduction, the LSLO's main task is to provide a large field of view image of the retina, so that the location of the AO-SLO image can be better determined. In addition, the overview image may facilitate subject alignment. Figure 3.1 shows the AO-SLO setup and its main components.

In brief, the system contains the AO part (SH-sensor, DM, control software) and the cSLO imaging part. Imaging and wavefront sensing is done with the same light (emitted from the SLO) at 840nm with a bandwidth of $\sim$ 50nm. 2D scanning of the retina is achieved by a resonant and a galvanometer scanner respectively. The backscattered light from the retina is detected by an avalanche photo diode. The field of view of the instrument is $\sim 1^\circ \times 1^\circ$, an image frame ($1250 \times 552$ pixels) is recorded in $\sim$ 69ms. This yields a frame rate of $\sim$ 14.6 frames per second. More details of the setup can be found in [24].

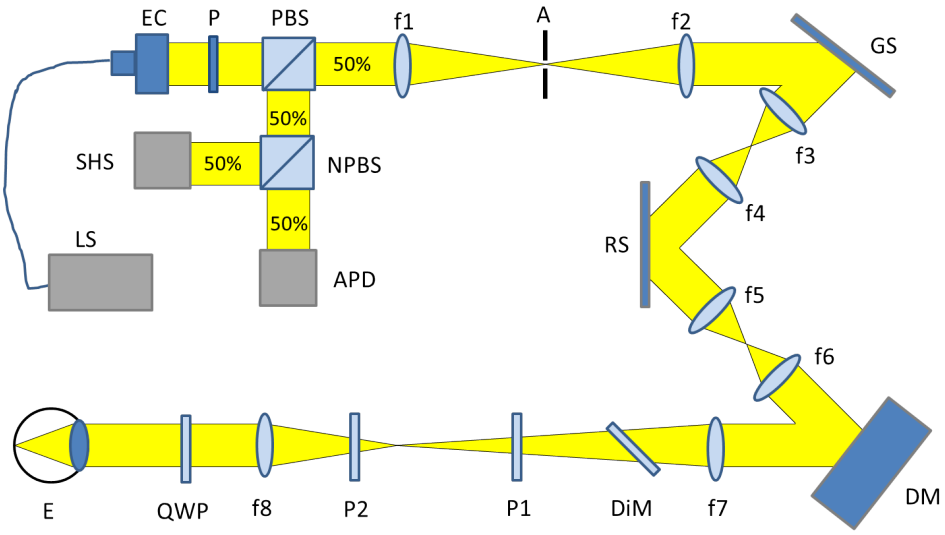

Figure 3.1: Scheme of the AO-SLO experimental setup [24]. LS: Laser source, EC: Entrance collimator, P: Polarizer, PBS: Polarizing beam splitter, $f_1 - f_8$: achromatic lenses, A: Aperture, GS: Galvo scanner, RS: Resonant scanner, DM: Deformable mirror, DiM: Dichroic mirror, P1-P2: Prisms, QWP: Quarter wave plate, E: Eye, SHS: Shack-Hartmann sensor, APD: Avalanche photo diode. Adapted from [24].

3.2 Design of the LSLO

In order to minimally influence the AO-SLO measurements, the LSLO is operated at 1050nm. The beam in the LSLO does not have to be corrected for aberrations introduced by the eye optics, because a low transverse resolution is sufficient (compared to the AO-SLO). Therefore both imaging beams are combined after the AO-SLO beam is reflected on the DM. Since both instruments are operated at different wavelengths a dichroic mirror (DiM) can be used (cf. Fig 3.1) for this purpose. The AO-SLO patient interface should not be changed, therefore the DiM was placed directly after lens f_7 in the setup. With this configuration some specifications of the LSLO are pre-determined (as will be explained later on). The design of the LSLO is shown in figure 3.2. The target specifications of the system were:

- Scanning the retina with an illuminating line with a maximized horizontal extension in order to obtain the broadest field of view as possible.
- The height of the illuminating line at the cornea should be approximately $\sim 1mm$ in order to achieve a reasonable transverse resolution.
- The given mechanical conditions (e.g diameter of lenses) and optical re-

strictions (e.g. specifications of the camera in the detection arm) of available components should be fulfilled.

Details on the LSLO specifications will be explained in sections 3.3.1 and 3.3.2.

3.2.1 Available Components

In the following the different parts of the system are explained.

Light source

The LSLO uses an amplified spontaneous emission (ASE) light source by NP Photonics with a central wavelength of 1050nm and a spectral width of 65nm Figure 3.3 shows the spectrum of the light source, table 3.1 summarizes its main characteristics.

Table 3.1: Main characteristics of the ASE light source [25]

Wavelength range [nm]	1000 - 1065
Output Power [mW]	> 20
Degree of Polarization [%]	< 5

The used infrared light source has three major advantages: Laser safety regulations allow higher exposure levels on the retina using longer wavelengths [26], since the delivered energy is inversely proportional to the wavelength. Higher exposure levels yield a higher signal to noise ratio. Second, infrared light sources are less absorbed by the photopigments of the eye than light sources within the visible light spectrum. Therefore, a bleaching of the retina is prevented. Furthermore, the patients' comfort is increased by the use of an invisible light beam because the subjective perception of the light intensity is much lower than for visible light. [25].

Galvanometer scanner

In the LSLO system, a GVS011/M Galvo scanner by Thorlabs Inc. is used which is responsible for moving the horizontal illumination laser line in vertical direction. The driving signal (saw tooth) for the scanner is generated by a field-programmable gate array (FPGA). For synchronization with the AO-SLO, the synchronisation signal of the resonant scanner is used. Thus, each

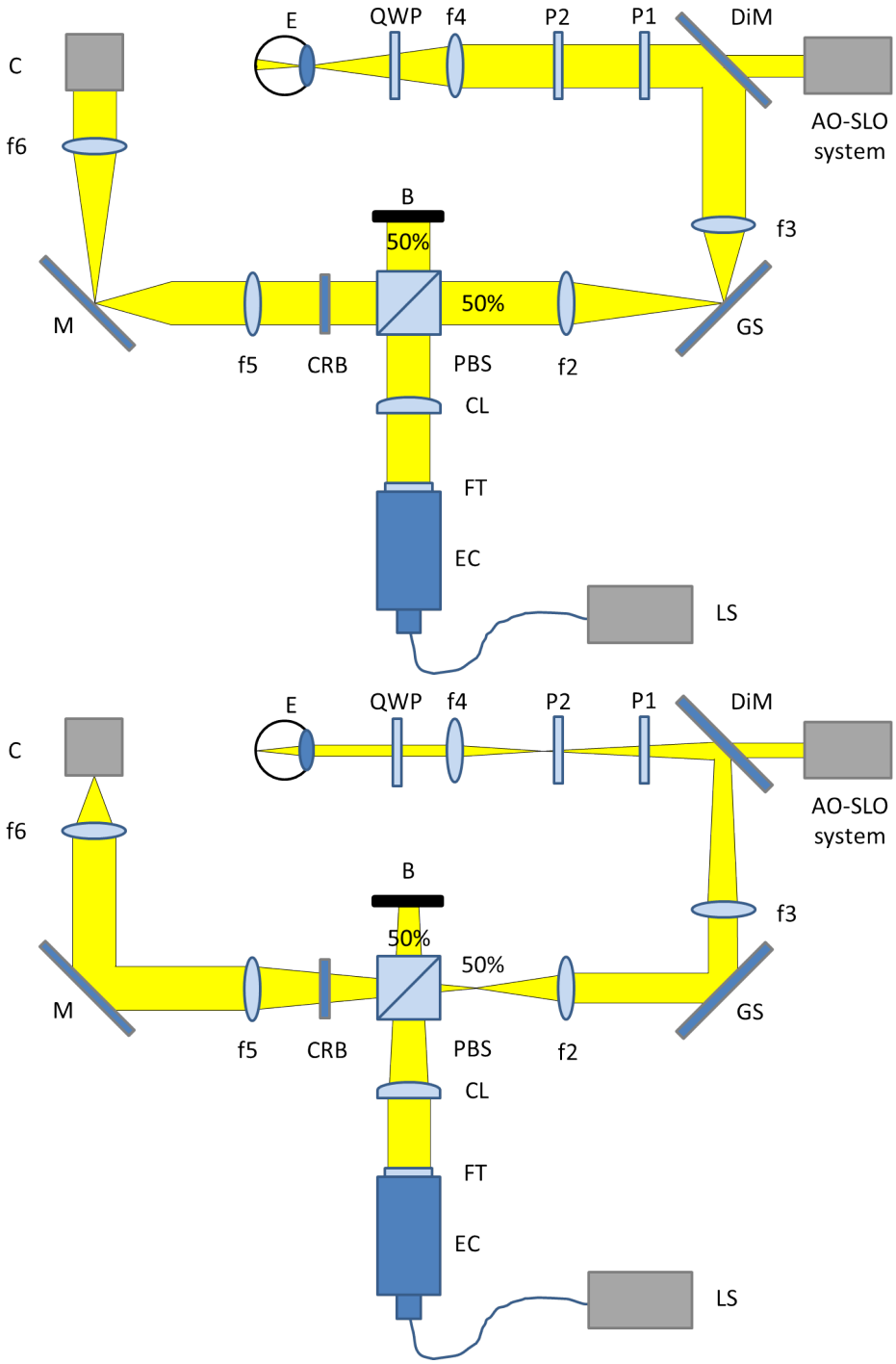

Figure 3.2: Scheme of the experimental setup of the LSLO in the horizontal (top) and the vertical (bottom) plane. LS: Light source, EC: Entrance collimator, FT: Neutral density filter, PBS: Polarizing beam splitter, B: Beamstop, CL: Cylindrical lens, $f_2 - f_6$: achromatic lenses, GS: Galvo Scanner, DiM: Dichroic mirror, QWP: Quarter wave plate, E: Eye, CRB: Aperture in order to block corneal reflections, M: Mirror, C: Line-scan camera.

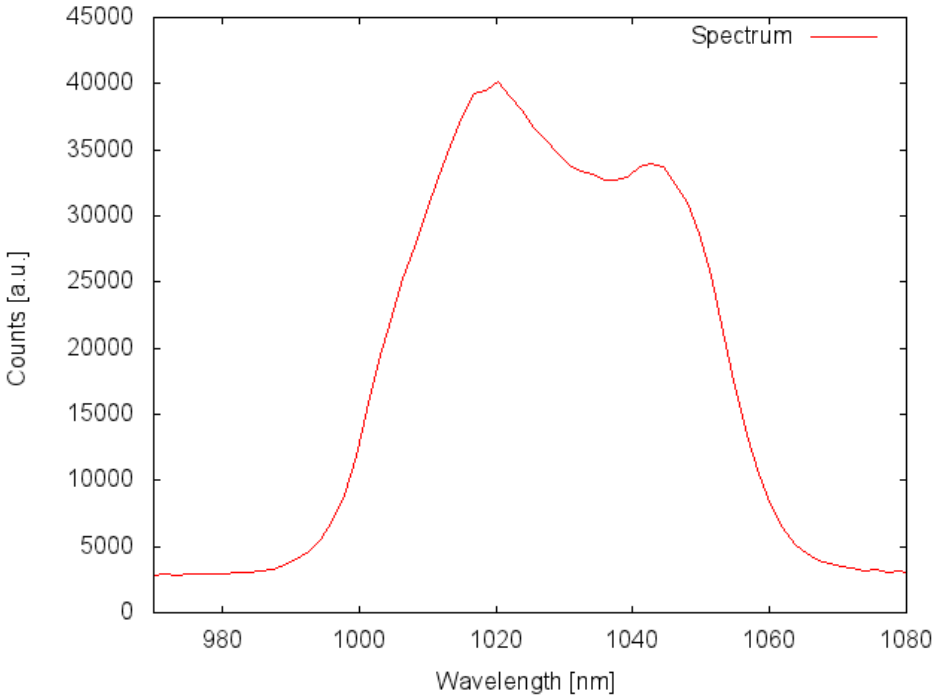

Figure 3.3: Wavelength spectrum of the ASE light source emitted from a single mode fiber

new AO-SLO line corresponds to a new line of the LSLO. Table 3.2 shows the specifications of the Galvo scanner in the LSLO system.

Table 3.2: Main characteristics of the Galvo scanner [27]

Reflectivity of mirror [%]	> 98
Maximum scan angle [°]	20.0
Small angle step response [μs]	400
Typical Resolution [°]	0.0008° (15μrad°)
Average Galvo Current [A]	1

Camera

For the LSLO, a 92kHz InGaAs linescan camera made by SUI, Goodrich Corporation was available. Table 3.3 shows the specifications of the used LSLO camera [28]. Note that the pixel height of the camera is not ideal for a LSLO. A smaller pixel height would be preferable.

Table 3.3: Specifications of the InGaAs linescan camera

Sensor format	1024 pixels at 12 bits
Pixel pitch [μm]	25
Optical aperture [μm]	500
Peak quantum efficiency [%]	> 70
Full well capacity [Me^-]	2.0
Nominal FPA sensitivity [e^-/counts]	450
Line rate [lps]	91.911

3.2.2 Beam propagation within the LSLO

In order to illuminate the retina with a line and to image the backscattered light onto the camera, additional optical elements such as lenses and mirrors are needed. This part briefly describes these elements and their respective tasks.

Entrance collimator

The light from the light source is delivered via a single-mode fiber. In order to collimate the beam, the fiber is connected to the entrance collimator (EC) with a numerical aperture (NA) of 0.1 and a focal length of f_c=25mm.

Neutral density filter

Power measurements on the emitted beam indicate that the total power on the retina will surpass laser safety regulations. Hence, a neutral density filter was installed directly after the collimator which reduces the incident power by 7 dB and yields a power of 1046μW at the cornea.

Polarizing beam splitter

A Polarizing Beam Splitter (PBS) is used in the LSLO system in order to construct an optical circulator. This yields an increase of the collection efficiency for the light returning from the retina. The PBS has three effects:

- The incident power is reduced by 50%.
- The incident light beam is refracted perpendicularly to its incident direction.
- The incident light beam is polarized.

In a first version of the LSLO setup, a 92%-8% Pellicle (P) was used instead of the PBS. In this setup, numerous image artifacts caused by reflections on lenses and other parts strongly lowered the image quality. Using a PBS, the incident light beam is linear polarized when traversing the PBS after the cylindrical lens at first. The quarter wave plate (QWP) located after the last lens f_4 subsequently transforms the linear polarized light into circular polarized light. The backscattered light from the retina traverses the QWP a second time which is then in a linear state that is orthogonal to the incident polarization state. Since back-reflections remain in the original polarization state, the light is reflected at the PBS and thus does not reach the detector. In contrast, the light from the retina traverses the PBS without being reflected and consequently enters the camera arm. Thus noise caused by backscattered light from lenses is suppressed.

Lenses

The location of the cylindrical lens and the achromatic lenses within the LSLO are shown in figure 3.2. All lenses are coated for near infrared light to optimize the optical throughput. Table 3.4 shows the list of lenses and their respective focal lengths.

Table 3.4: Lenses in the LSLO

Lens	**Focal length [mm]**
f_{CL} (Cylindrical lens)	200
f_2	80
f_3	400
f_4	180
f_5	80
f_6	400

Sections 3.3.1 and 3.3.2 give more information on the design of the lens system.

Dichroic mirror

The dichroic mirror (DiM) is used to combine the beams of the LSLO and the AO-SLO systems and is oriented at 45° in respect to the incident beams. Light consisting of wavelengths that are longer than 1000nm are reflected,

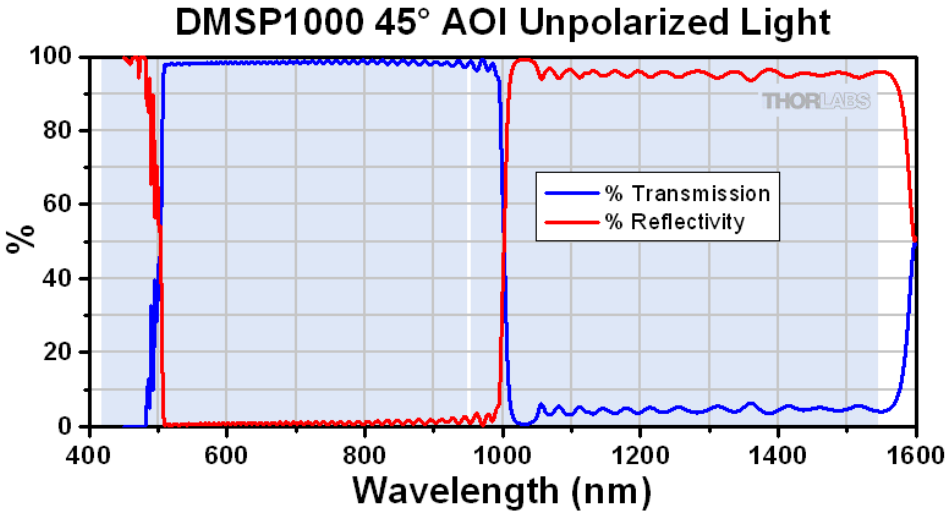

Figure 3.4: Transmission and reflectivity spectra for the DiM. Source: `http://thorlabs.com`

whereas light consisting of shorter wavelengths is transmitted. Consequently, it can be regarded as a mirror for the LSLO beam ($\lambda_L \sim 1050nm$). The AO-SLO beam ($\lambda_{AO} \sim 850nm$), however, traverses the DiM. Figure 3.4 shows the transmission and reflection spectra of the DiM.

Prisms

Two prisms reflect the vertical beam after the DiM and change the direction of the beam into a horizontal plane before the beam traverses the last illumination lens f_4 of the system.

Corneal reflections blocker

Reflections from the cornea (see chapter eye) might create image artifacts on the retinal image. Therefore, a stripe was placed in front of the first camera arm lens f_5 in order to block the corneal reflections. The stripe is a simple piece of plastic strip that is large enough to block corneal reflections, while the light from the retina is marginally affected.

Other parts

All components are mounted on an optical table with posts, post holders and clamps. In addition, a mirror is placed between the lenses f_5 and f_6. This yields a folding of the beam propagation which optimizes the use of the limited space on the optical table.

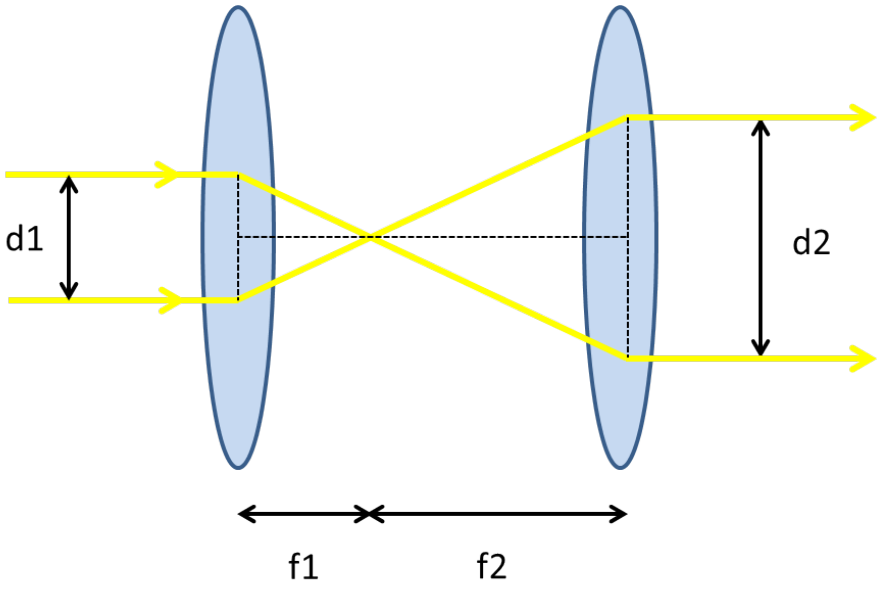

Figure 3.5: Schematic of beam diameter magnification using telescopes

3.3 Design of the LSLO imaging optics

The LSLO requires a line illumination of the retina. On the other hand, the light backscattered from this line has to be imaged onto the line-scan camera. The used camera and the last lens that is shared with the AO-SLO system already define fixed conditions for this LSLO. In addition, the imaging optics have to image the pivot point of the scanner onto the pupil plane of the eye to enable 2D scanning of the retina. Another fixed condition was the available entrance collimator which provides a beam diameter of $\sim$ 5mm. The setup consists of a PBS, one cylindrical lens (CL) and five achromatic lenses. The cylindrical lens breaks the radial symmetry of the system. Therefore, in order to better illustrate the beam propagation, two different planes of the setup (horizontal and vertical) have to be shown (cf. figure 3.2). For better visualization, the setup is split into the illumination optics (cf. figure 3.7) and the camera detection optics (cf. figure 3.8).

Beam magnification and de-magnification can be achieved using telescopes consisting of two lenses with different focal lengths f_1 and f_2 that are separated by a distance of L=$f_1 + f_2$. Figure 3.5 illustrates the principle of beam magnification. Using the intercept theorem, we obtain: $d_2 = d_1 \cdot \frac{f_2}{f_1}$ [29].

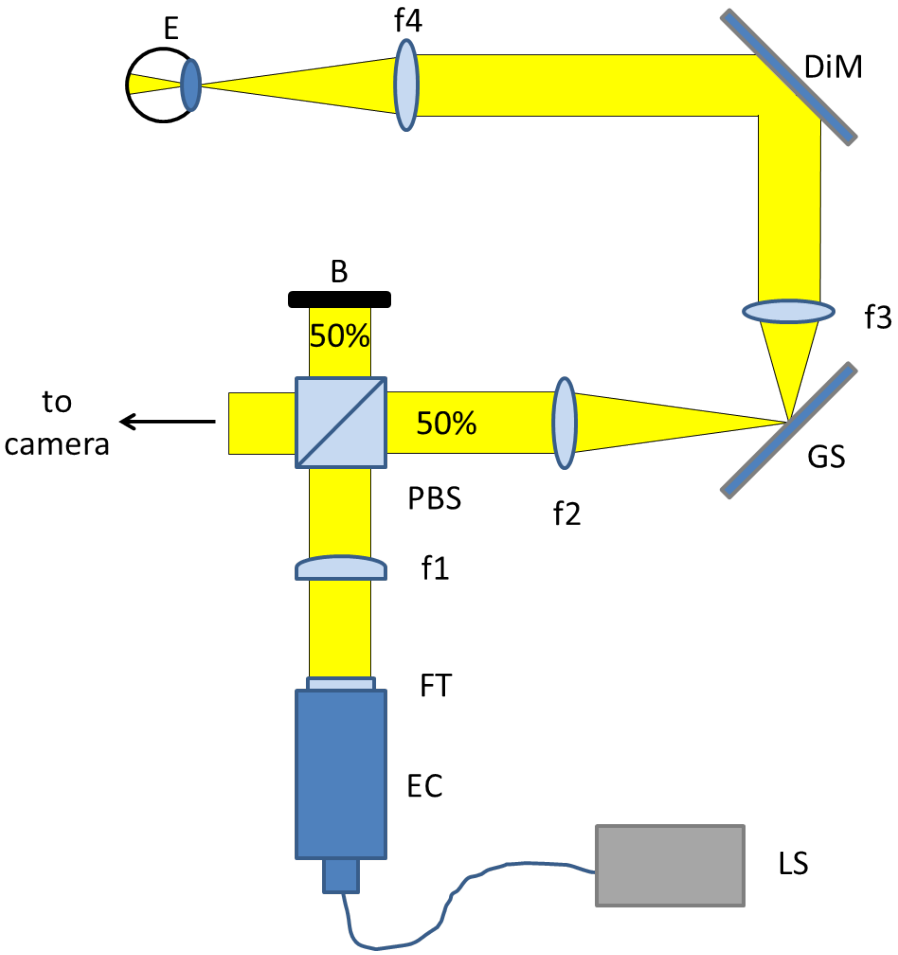

Figure 3.6: Scheme of the illumination optics. LS: light source, EC: Entrance collimator, FT: Filter, PBS: Polarizing beam splitter, B: Beam stop, CL: Cylindrical lens, $f_2 - f_4$: achromatic lenses, GS: Galvo Scanner, DiM: Dichroic mirror, E: Eye

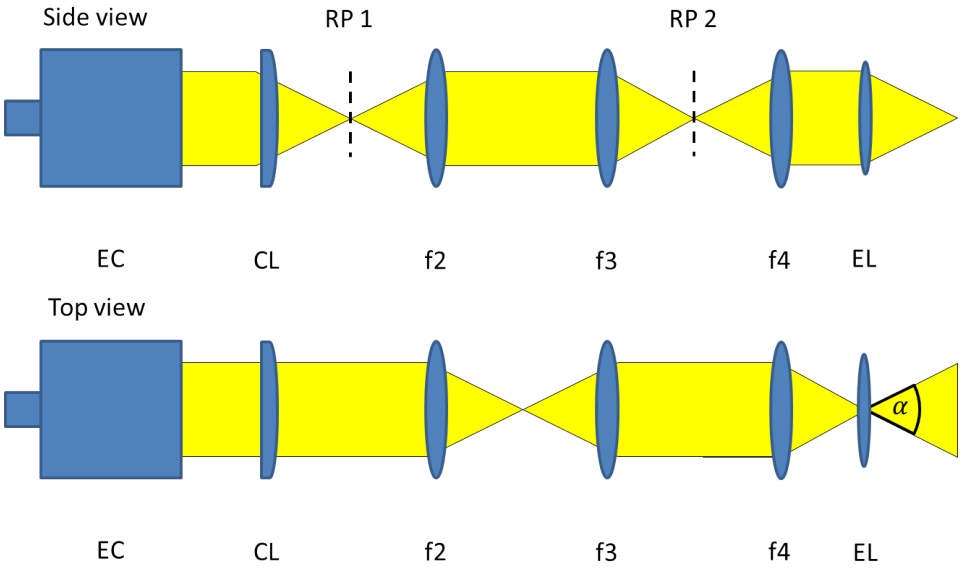

Figure 3.7: Beam propagation from side view and top view in the illumination arm (reflections by 90° occurs at the Galvo scanner and the DiM are omitted for clarity). EC: Entrance collimator, CL: Cylindrical lens, f2-f4: Achromatic lenses, EL: Eye lens, RP 1 / RP 2: Conjugates to the retina plane, α: scanning angle

3.3.1 Design of the illumination arm

The collimated beam firstly traverses the cylindrical lens, thus the beam profile is focused in vertical direction at the focal plane of the cylindrical lens and stays collimated in the horizontal plane. Then the beam traverses the PBS where light is split into the two orthogonal polarization states. One part is reflected by the PBS while the other is transmitted. Since the light emitted by the light source is un-polarized, 50% of the light intensity is reflected and traverses the following lens f_2. The distance between the cylindrical lens and f_2 corresponds to the sum of the two focal lengths. Subsequently, the beam is collimated again in the vertical plane and focused in the horizontal plane. Then, the beam hits the GS that is placed in the focal plane of the f_2 lens at its pivot point and the beam is deflected perpendicular to its incident direction. The lens f_3 refocuses and recollimates the beam in the horizontal and vertical directions respectively. The DiM deflects the beam again and combines the AO-SLO beam with the LSLO beam so that both beams overlap and share the same propagation direction. Finally, the beam is collimated and focused again by the lensf_4 in the vertical and horizontal plane respectively before it is sent to the eye.

Now the question arises how to choose the focal lengths for each lens. In order to solve this question, calculations and MATLAB simulations were performed. Several fixed conditions and additional criteria have to be taken into account:

Fixed conditions for the lens system simulations:

I The last lens f_4 has a focal distance of f_4=180mm, because this lens is shared with the adaptive optics system which should not be altered.

II The diameter of the last lens is 4cm.

III The NA of the available entrance collimator is fixed.

Additional criteria for the lens system simulations:

1. The horizontal angle α of the beam after lens f_4 defines the scanning area and therefore the field of view of the LSLO. This angle should be maximized
2. The vertical height of the beam at this location defines the transverse resolution perpendicular to the line. This should be $\sim 20\mu m$ which corresponds to a vertical height of $\sim$ 1 mm at the cornea.
3. Only standard lenses should be used that are available for a reasonable price on the market.

Taking into account the fixed conditions, the beam diameter d of the incident beam needs to be calculated. With an effective numerical aperture (NA) of NA=0.11 [30] of the single-mode fiber and a length of l=2.5cm of the EC, we obtain [31]:

With

$$d = 2 \cdot NA \cdot l = 5.5mm \tag{3.1}$$

As specified by the manufacturer, this beam diameter d correponds to the width of a gaussian beam profile measured as the distance between points of the profile where the intensity has dropped to $1/e^2$ of the peak intensity [31]. The numerical aperture is defined as:

$$NA = n \cdot sin(\phi) \tag{3.2}$$

Where n=1 corresponds to the refraction index of the surrounding medium of the single-mode-fiber (in our case n=1 for air) and ϕ to the divergence angle of the beam exiting the fiber. Using equation 3.1, we can calculate the beam angle α and height d_y of the line at the cornea:

$$tan(\frac{\alpha}{2}) = \frac{d_x}{f_4} = d \cdot \frac{f_3}{f_2 \cdot f_4} \tag{3.3}$$

$$d_y = d \cdot \frac{f_2}{f_{CL}} \cdot \frac{f_4}{f_3} \tag{3.4}$$

Since we have 3 unknowns (f_{CL}, f_2, f_3) and only two equations we have one degree of freedom to choose our components. Therefore different configurations were simulated using MATLAB together with the incident beam diameter d=5.5mm (3.2) and equations (3.3), (3.4). Following possible focal distances were included in the simulations:

Table 3.5: Focal distances of achromatic lenses included in the simulation of the illumination path optics.

Focal distance [cm]	7.5	8	10	15	20	25	30	40	50

Table 3.6: Focal distances of the cylindrical lenses included in the simulation of the illumination path optics.

Focal distance [cm]	2.5	5	6	7.5	8	10	13	15	20	25	30	40	50

The simulation performs the calculation of the beam angle and beam height in y-direction for all focal distances given in tables 3.5 and 3.6. From these results, only combinations that surpass a given limit for the scanning angle α and the beam height d_y are selected. Usually, this gives about 20 combinations that are within the specified range.

From this list, we manually chose the most appropriate set of lenses using the following criteria in a strict order:

1. A large scanning angle α
2. A vertical beam height d_y as close as possible to $\sim$ 1mm

3. A length of the whole illumination optics that lies within the given spatial limits of the optical table with the AO-system.

Using these criteria, the following configuration was chosen:

- f_{CL}=200mm (cylindrical lens)
- f_2=80mm
- f_3=400mm
- f_4=180mm (given)

With this set of lenses, we obtain a theoretical line width of $d_x = 27.5mm$ and a height $d_y = 0.99mm$ which yields a field of view angle of $\alpha = 8.69°$. Assuming that 1° scanning angle corresponds to $300\mu m$ on the retina, a $\sim$ 2.6mm field of view on the retina is achieved with this configuration. With

$$\Delta y = 1.22 \cdot \lambda \cdot \frac{f_{EL}}{d_y} \tag{3.5}$$

the transverse resolution on the retina can be calculated to $\Delta y \sim 28\mu m$, where $f_{EL} = 22mm$ corresponds to the average eye length.

In a second step, the influence of the numerical aperture on the lens configuration was investigated. Here only commercially available single-mode fibers and ECs were considered. With an EC of 5cm focal length and a NA of 0.14 the following configuration was obtained:

- f_{CL}=500mm (cylindrical lens)
- f_2=100mm
- f_3=200mm
- f_4=180mm (given)

Table 3.7 compares the results for the beam height and incident angle for both collimators. As can be clearly seen, changing the NA and the focal distance of the EC will mainly change the beam height of the incident light. Using a higher NA of the collimator will increase the transverse resolution in y-direction on the retina. However, The overview LSLO will not be corrected with AO and aberrations will degrade the image quality. Therefore the lower transverse resolution as provided by the first configuration was chosen.

Table 3.7: Simulation results of the beam diameter in the y-direction and the scanning angle α for two different ECs.

NA EC []	**Focal length EC [mm]**	**Height [mm]**	$\alpha[^\circ]$
0.11	25	0.99	7.69
0.14	5	2.52	8.84

In order to increase the beam angle (and therefore the FOV) on the retina, the last lens f_4 has to be exchanged. In order to investigate the influence of a lens with a shorter focal distance and larger diameter, simulations were performed for a standard lens with a focal distance f_4=100mm and a diameter of 2 inch (5.08cm) (cf. table 3.8). 3.8.

Table 3.8: Simulation results of the beam angle α and diameter using a NA=0.11 for a configuration with a lens f_4=100mm and a lens diameter of 5.08cm.

Width [mm]	**Height [mm]**	$\alpha[^\circ]$
35	0.93	19.29

Indeed, exchanging the last lens would result in a better scanning angle and thus strongly increase the FOV. However, the last lens f_4 cannot be altered because this would require a re-design of the AO-SLO system.

3.3.2 Design of the detection optics

With the lens settings from the illumination path, the first part of the detection path is determined. In order to adapt the image for an optimum usage of the camera, additional optics are needed.

The pixels of the camera have a rather large height (500 μm). Therefore, the focusing of the line onto the camera is not very critical. Let us then consider the magnification that is needed for an optimum usage of the full line length of the camera. The line-scan camera consists of 1024px with a pixel pitch of 25 μm which yields a total camera width of $d_{max} = 25.6mm$.

Figure 3.8 illustrates the beam propagation from the PBS to the camera.

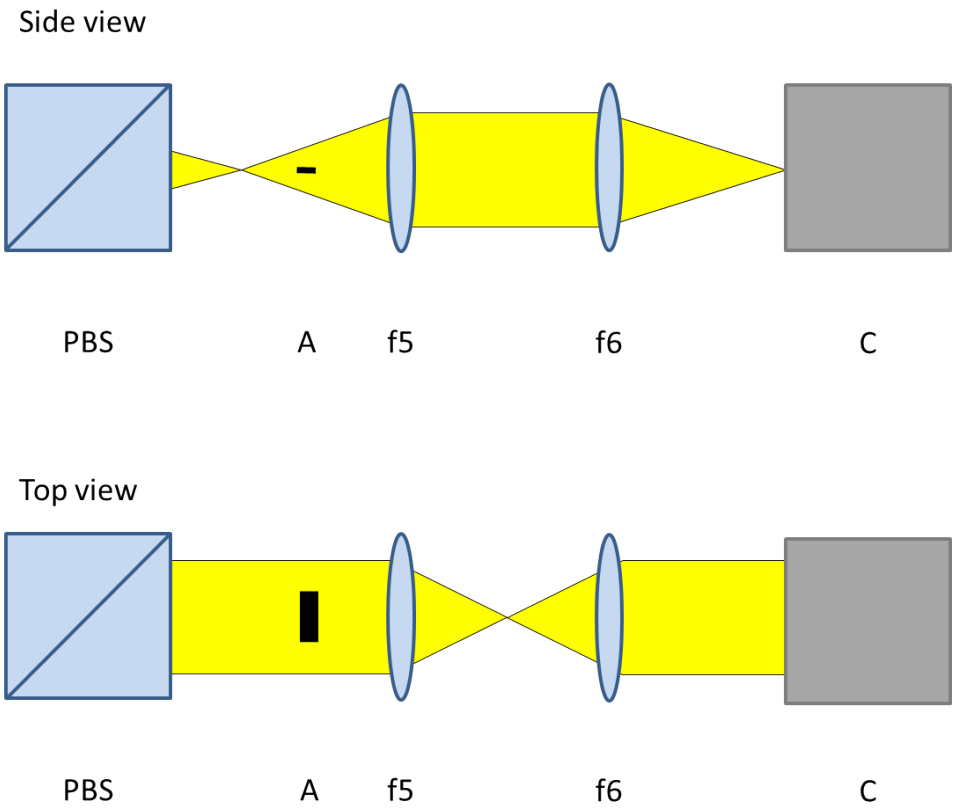

Figure 3.8: Side view and top view of the beam propagation from the PBS to the line-scan camera. PBS: Polarizing beam splitter, A: Aperture to block corneal reflections, f5-f6: Achromatic lenses, C: Camera

The horizontal beam width at the PBS (see figure 3.2) corresponds to the incident beam width diameter $d = 5.5mm$. Using two lenses for imaging the line onto the camera, we obtain following relation between d_{max} and d: $d \cdot \frac{f_6}{f_5} \leq d_{max}$.

By choosing following focal lengths for the lenses,

- f_5=100mm
- f_6=400mm

this condition would be fulfilled. We obtain a theoretical lateral beam width on the camera of $d_c = 22mm$, which is below the total length of $d_{max} = 25.6mm$. However, the used prisms in the illumination path cut off a small portion of the total illumination line which results in a smaller line length returning from the retina. Therefore, a lens with a focal distance of f_5=80mm lens was chosen instead. Thus the horizontal line width returning from the retina is optimally imaged onto the full length of the camera. In order to correct defocus of the imaged eye, lens f_5 is mounted on a translation stage. The beam height on the last focusing lens f_6 is calculated with 2.01mm which results in a focus on the camera of 232μm (using eq. 3.5) which is smaller than the vertical pixel size of the camera.

3.4 Alignment process

Before starting the alignment process, several fixed conditions need to be considered. As a first step, the positions for all the lenses, the scanner and the camera need to be determined.

The lenses need to be separated by the sum of their focal lengths in order to ensure that the beam is still collimated in y-direction when illuminating the eye. In addition, the pivot point of the scanner has to be imaged onto the pupil plane of the eye. This yields distances between the lens positions in the illumination arm shown in table 3.9:

Similarly, we obtain the distances between the lenses for the camera arm (cf. table 3.10).

Table 3.9: Distances between the lenses and the GS for illuminating the retina. f_{CL}=200mm corresponds to the cylindrical lens, f_2=80mm, f_3=400mm, f_4=100mm.

Lens	CL	f_2	GS	f_3	f_4
Distance [mm]	280	80	400	500	

Table 3.10: Distances between the lenses and the camera in the camera arm. f_2=80mm, f_5=80mm, f_6=400mm.

Lens	f_2	f_5	f_6	C
Distance [mm]	160	480	400	

Between f_6 and the camera, the laser beam is collimated in the horizontal direction but not in the vertical direction. Hence, we need to place the camera in the focus plane of f_6. One additional condition for the setup are spatial limits on the optical table because on the table the AO system and a OCT system are already set up. Figure 3.9 shows an overview scheme of the systems on the optical table together with the location of the LSLO setup. With the pre-determined distances along the beam propagation, one degree of freedom, the vertical distance of the system from the table surface, remains for the setup. This height can be chosen freely in order to meet the restrictions set by other components on the optical table. Once this distance is found, the components (all lenses, the GS, PBS) can be placed onto the table and are arranged on the optical table considering their respective positions.

The polarizing beam splitter is put between f_2 and f_5, close to the focus point of both lenses.

After this initial arrangement of the components, the system can be aligned. For laser safety reasons, a 20dB filter is placed directly after the EC in order to attenuate the light intensity. Then the light source is turned on and the collimation of the beam exiting the collimator is checked. This can be done with an IR-sensor card by observing the beam size at several distances from the EC. The beam size should not change over a distance of several meters. Otherwise, the EC has to be adjusted in order to meet this criterion. In addition, the shape of the beam profile can be checked. The beam profile should have a Gaussian shape, otherwise the single-mode fiber has to be cleaned or replaced. In order to measure the size of the beam exiting the EC, the beam profile was recorded with a WinCamD Series camera by Dataray Inc. With the software that was delivered with the camera, an effective beam diameter

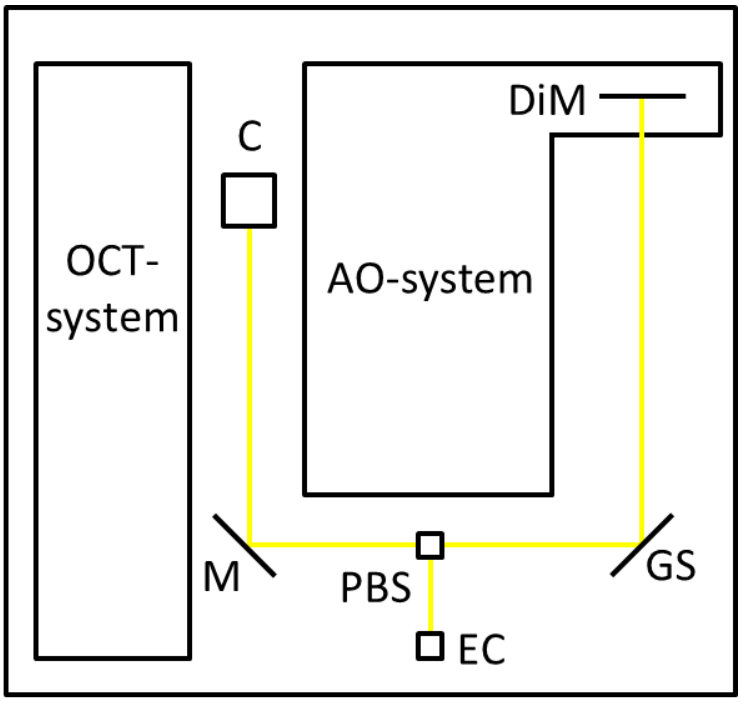

Figure 3.9: Scheme of the systems on the optical table and the implementation of the LSLO. EC: Entrance collimator, PBS: Polarizing beam splitter, GS: Galvo scanner, DiM: Dichroic mirror, C: Camera

of 5291 μm was measured.

In the next alignment step, the direction of the collimated beam needs to be adjusted. The beam should be parallel to the optical table, and parallel to the drilling holes of the optical table. First the height of the collimator is adjusted to the height of the system. Then the collimator mount is tilted until the beam is parallel to the drilling holes of the optical table. To check this alignment, all lenses and the PBS are removed from their post holders. In a next step, the PBS is inserted into the system and the beam location on the PBS is checked with an IR-sensor card. The beam that is reflected by the PBS should remain parallel to the optical table, and propagate perpendicular to the incident beam. This is similarly checked by measuring the height and the location of the beam at different distances from the PBS. After this alignment, the GS is inserted in a way, that the beam hits the GS on the pivot point and is reflected in orthogonal direction to the incident beam, but remains parallel to the optical table. In a next step, the DiM is aligned to ensure that the AO-SLO and the LSLO beams propagate into the same direction. Then, the quarter wave plate (QWP) is inserted into the system. The QWP is oriented

at 45° to the incident polarization plane and converts the linear polarization state into a circular polarization state. After inserting the QWP, a mirror is placed at the location of the eye and the angle of the mirror is adjusted until the beam is reflected in itself. Therefore, the backreflected beam traverses all components again until it reaches the PBS. Since the QWP is traversed a second time, the polarization state of the light is now linear but orthogonal to the incident polarization state. Thus the beam is not reflected by the PBS and enters the detection arm. In this arm the components (two lenses, f_5 and f_6, and a fold mirror) are placed in such a way that the reflected beam hits these components centrally. The alignment of the height of the lenses has to be done very accurate, since small errors may cause huge deviation of the beam propagation.

The lenses in the camera arm are the first to be inserted, because in this way the position of the lenses can be aligned using the collimated beam returning from the mirror. After inserting the cylindrical lens this would be more difficult.

In a last step lenses in the illumination arm are inserted in a similar way. In order to take advantage of the collimated beam (which makes the alignment easier) the procedure is started with lens f_4 lens. Other lenses are then inserted in descending order (f_3 to f_1). Table 3.11 and 3.12 illustrate the components and their distances to the previous component in the illumination and the camera arm.

Table 3.11: Components and their distances to the previous one in the illumination arm. Measurements were performed from the centers of the components

Component	**Distance to previous component [cm]**
EC (with fixated filter)	
f_1	1.5
PBS	21
f_2	7
GS	8
f_3	40
Dichroic Mirror	19.5
First Prism	14.5
Second Prism	14
f_4	10
EL	18

Table 3.12: Components and their distances to the previous one in the detection arm. Measurements were performed from the centers of the components

Component	**Distance to previous component [cm]**
PBS	
f_5	9
Mirror	23.5
f_6	24.5
Camera	40

Chapter 4

Software

During this thesis control software for the camera and the galvo scanner had to be developed. For this purpose, LabView virtual instruments from National Instruments was used. This section briefly explains different tasks of the control software and parameter which have to be set by the operator of the LSLO.

4.1 Camera control

The camera control software was developed in order to set different camera parameter and to provide an online display of the acquired images. In addition the images may be recorded on a hard disc using this program. The different camera parameter (e.g. exposure time) can be set with the program LSLO-camera.vi. This program was developed using the IMAQ (image acquisition) package for LabView. The program establishes a connection with the camera and subsequently sets several parameters such as image type, image size and trigger mode. After setting of these parameters, continuous data acquisition is started. For the online display the acquired images are extracted from the camera buffer and displayed. In addition, the program provides the option to stream the data on a hard disc.

Following parameters have to be set by the user:

- Exposure time [μ s]: For in-vivo measurements 353.9μs or 125.0μs were used. The typical exposure time for the model eye was also set to 125.0μs. With a the corresponding number of scanning lines of 1400 (for 353.9μs) and 550 (for 125.0μs) we can calculate a frame

rate of ~ 5.7 and ~ 14.6. frames per second (FPS) while scanning with 1400 and 550 lines respectively.

- Sensitivity: A setting of 450[e-/count] is required for in-vivo measurements and recommended for artificial eye measurements.
- Filename: With this name files are saved on the hard disc. Different names can be chosen for snapshots and streams. Snapshots are saved as ".tif" images directly, streams are exported as ".raw" files. These ".raw"-files consist of a 4×16-byte header containing the frame width and height (1024×1000 in our case) and a zero value after each parameter. Furthermore, the file contains $1024 \times 1000 \times Number\ of frames$ of 16byte signed values in order to clearly define the grayscale stream.
- Trigger mode: For the measurements "Trigger each buffer" was used.
- Digital gain: Usually this parameter was set to 2 for in-vivo and model eye measurements. In order to measure the signal to noise ratio on the model eye, a digital gain of 1 was used. This is due to the saturation limit which is reached because of the high signal level in the model eye when using a digital gain of 2.
- Byte order: Big or little endian for the stream data files.

4.2 Scanner control

The scanner control software allows the user to set the amplitude of the LSLO galvo scanner and the number of scanning lines (which depends on the frequency of the scanner). In order to control the GS, a field programmable gate array (FPGA) is used which provides the necessary analog output voltages and the corresponding trigger signals for the camera control. The FPGA is already implemented into the AO-SLO system. The "master" clock of the AO-SLO is the resonant scanner which operates at 4kHz. The same clock is used in order to generate the corresponding signals for the LSLO. The program is named ScannerControl.vi

The amplitude of the scanner is set in arbitrary units and has to be converted into voltage units in order to set the corresponding scanning angle of the

GS. The number of lines set in the program determines the scanner frequency and frame trigger of the LSLO (i.e. the trigger that is sent at the beginning of a new 2D image and correspond to the back setting of the scanner). The scanner control software is operated on a different computer and is independent from the camera control software (cf. previous chapter). The frame grabber of the camera receives the corresponding trigger signals. However, the exposure time of the camera has to be set accordingly in order to fit into the scanning protocol of the GSs. Otherwise the image frame will not be triggered correctly. Note that for correct triggering both scanner frequencies (AO-SLO and LSLO galvo scanners) have to be the same and the values have to be set before the FPGA program is started.

4.3 Display of recorded data

After recording of data a separate program is used for data display. This can be done with the program LSLOread-out.vi. This program additionally enables image-averaging of a recorded stack in order to improve the SNR. The basic function of the program is to transform the read-out data into an appropriate image stack. Individual images are displayed and the user may look through each of the recorded images. Images that show poor image quality can be removed by a simple mouse click from this block. For frame averaging, the user has to select one image as reference frame. This frame should show good image quality and no motion artifacts. Then a cross correlation algorithm is applied in order to correct a translation (caused by transverse motion) between the individual image frames. After this correction all frames are averaged. In some cases it can be advantageous to calculate the cross correlation only in a region of interest (ROI) and apply the translation to the whole image frame. Therefore the user has the possibility to choose this ROI before applying the cross correlation algorithm to the whole image frame which improves the averaging result.

Chapter 5

Characteristics of the LSLO

In this chapter, the main characteristics of the LSLO system such as light power losses, spectral throughput, sensitivity or signal-to-noise ratio are addressed.

5.1 Light power losses within the LSLO system

In order to check the losses within the system, the light power was measured with a powermeter (Thorlabs PM100D) at different locations of the system. The emerging power from the light source was measured with 20.86mW.

Table 5.1 summarizes the power measurements at different locations within the setup. The main losses are introduced by an auxiliary fiber, the 7dB neutral density filter and the polarizing beam splitter. The auxiliary fiber was inserted between EC and the fiber which is attached to the light source. This was necessary because the fiber tip from the light source was damaged and did not provide a Gaussian intensity profile. Since the power from the light source is too high and needs to be attenuated the insertion of the auxiliary fiber was chosen. Traversing lenses and reflections at the mirrors cause rather small losses. Since the beam is broader than the detector size of the powermeter, locations between f_2 and f_4 have not been included into these measurements.

5.2 Spectrum

Figure 5.1 shows the wavelength spectrum of the beam emitted by the light source (LS) (before entering the LSLO system) and at the location of the eye (after traversing the whole lens system). We can observe a slight decrease in

Table 5.1: Power measurements of the light beam in the LSLO setup

Position	**Power [μW]**	**Remaining Power [%] to previous location**
LS output	20860	
After single mode-fiber	10980	52.6
After EC	10970	99.9
After filter	3074	28.0
After f1	3034	98.6
After PBS	1369	45.1
After f2	1355	99.9
After f4	1081	79.8
Total		**3.9**

the spectral width of the spectrum of the light that traversed the system. This may be caused by the DiM. The cut off wavelength for the DiM is (cf. figure 3.4) around 1000nm. Therefore parts of the shorter wavelength spectrum is not reflected by the DiM which results in the observed loss of spectral width. However, for the LSLO preservation of the spectral width is not critical.

5.3 Sensitivity

Sensitivity measurements were performed by placing a mirror at the intended location of the eye. The mirror was aligned so that the beam was reflected in itself. In order to avoid saturation of the camera, a 20dB filter was placed into the beam in front of the mirror, resulting in a power loss of 40dB (the beam passed the filter twice). However, the actual attenuation coefficient for the LSLO light source was measured to be 17.9dB with a powermeter (Thorlabs Inc.) Thus the power loss due to the filter was 35.8dB. In order to measure sensitivity the signal-to-noise ratio (SNR) was determined for this configuration. Equation 5.1 shows the definition of the SNR mathematically with S being the power of the signal within the images and N being the total noise of the camera at a given exposure time. The noise was determined by blocking the sample beam and calculating the standard deviation of the noise image.

$$SNR = 10 \cdot log\frac{S}{N}\ [dB] \tag{5.1}$$

Table 5.2 shows the sensitivity for several exposure times.

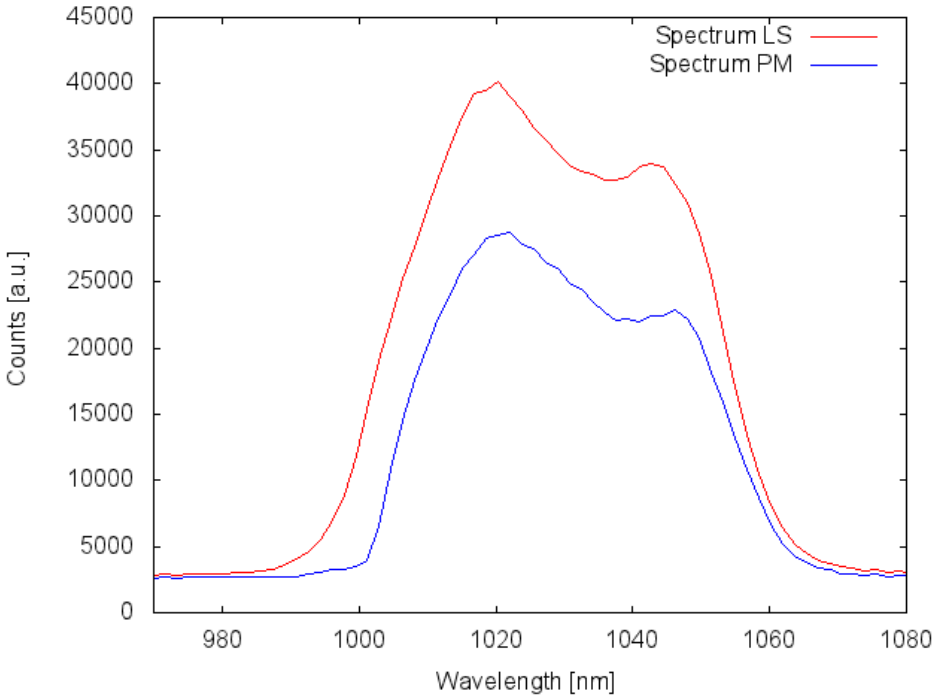

Figure 5.1: Wavelength spectrum of the beam emitted by the light source (LS) (before entering the the LSLO system) and at the location of the eye (after traversing the whole lens system).

Table 5.2: Sensitivity for different exposure times

Exp. time [μs]	**Signal [a.u]**	**Noise [a.u]**	**SNR [dB]**	**Sensitivity [dB]**
44.3	961	2.94	25.1533	60.9533
177	3685	2.91	31.0349	66.8349
353.9	4043	3.11	31.1498	66.9498

In a next step the theoretical expected sensitivity was calculated. First the minimum power that can be measured with the camera has to be determined. The camera's full well capacity (FWC) of $FWC = 2 \cdot 10^6$ electrons corresponds to 12 bits(4095) per pixel. Thus, we can calculate the number of electrons per pixel that corresponds to the digitization noise of the camera:

$$N_{el/pix} = FWC/4095 \tag{5.2}$$

Consequently, using the camera's peak quantum efficiency (PQE) of 70% we obtain the total number of photons that corresponds to one digit of the camera:

$$N_{phot} = \frac{N_{el/pix}}{PQE} \tag{5.3}$$

Hence, using Einstein's formula yields:

$$E = N_{phot} \cdot h \cdot \frac{c}{\lambda} \tag{5.4}$$

where h corresponds to Planck's constant $h = 6.6 \cdot 10^{-34}\ J \cdot s$, c to the speed of light $c = 3 \cdot 10^8\ m/s$ and λ to the system's wavelength of $\lambda = 1.05\ \mu m$. Having an exposure time $t = 353.9\ \mu s$, we can calculate the power equivalent for one digit of the camera:

$$P = \frac{E}{t} \tag{5.5}$$

Performing such calculations, we obtain for the minimum detectable power on the camera: $P_{min} = 0.37$pW whereas we obtain saturation of the camera at $P_{max} = P_{min} \cdot 4095 = 1.59$nW per pixel at an exposure time of $t = 353.9 \mu s$. The power returning from the sample (mirror) is approximately 1mW (neglecting losses introduced by the lenses). With a scanning line width on the camera of 955 pixels (see section 5.4), this yields a power of 1.05 μW and a theoretical sensitivity of

$$S = 10 \cdot ln(\frac{P_{returning}}{P_{noise}}) = 64.5\ dB \tag{5.6}$$

which is in good correspondence with the measured sensitivity.

Furthermore, signal-to-noise measurements were performed on the model eye (see below). Table 5.3 shows the sensitivity for several exposure times.

Table 5.3: Signal-to-noise ratio measurements on the model eye for different exposure times

Exposure time [μs]	**Signal [a.u]**	**Noise [a.u]**	**Signal to Noise [dB]**
44.3	2380	2.92	29.11194106
177	4046	2.87	31.49143982
353.9	4093	2.92	31.46658893

5.4 Calibration of the field of view

In order to determine the field of view provided by the LSLO, measurements on a sliding caliper were performed. To simulate the eye a lens with 30mm focal length was placed at the location of the sample. The sliding caliper was placed at the focal plane of the lens (location of the retina) and the distance between the arms was set to 1mm. With this configuration a LSLO image was recorded. After this measurement, the caliper was tilted by 90° in order

to determine the FOV for the vertical direction. From these images, lateral and transversal pixel widths of 122px/mm and 156px/mm were determined respectively. Thus length to pixel ratios of 3.93μm/px and 2.94μm/px in the x- and y- directions were obtained.

In order to determine the lateral resolution of the instrument in the model eye, the width of the edge of one arm of the caliper was measured. The measured 14px and 15px respectively correspond to a transverse resolution of 55μm and 44 μm respectively. With

$$\phi = 2 \cdot arctan(\frac{a}{2d}) \tag{5.7}$$

we can calculate the resolution in angular units, where a corresponds to the resolution and d to the focal distance of 30mm of the auxiliary lens. This yields $\xi_x = 0.41°$ and $\xi_y = 0.25°$. From the FOV and the size of the image (955 $\times$ 920 px) we can calculate the scanning angle ϕ using eq. 5.7 and the scanning width and height of $955 \cdot 3.93\mu$m and $920 \cdot 2.941\mu$m. Hence we obtain scanning angles of $\phi_x = 7.20°$ and $\phi_y = 5.16°$ in the x- and y directions respectively. $\phi_x = 7.20°$ is in good accordance with the prior calculated theoretical scanning angle $\alpha = 8.69°$ (see table 3.8). The deviation between the measured and the theoretical scanning angle $\phi_x = 8.69°$ is mainly caused by the limited size of the first prism which results in a cut-off of the imaging beam. Table 5.4 summarizes the calibration measurements.

Table 5.4: LSLO calibration measurements. Camera set at: Exposure time t=125.2μs, sensitivity: 450[e-/counts]. Scanner settings: scanning amplitude: 2000[a.u.], number of lines: 550.

	px/mm	**μm/px**	**Width [px]**	**Width [mm]**	**α[°]**	**Edge width [px]**
x	254	3.93	955	7.4	7.20	14
y	340	2.94	920	6.0	5.16	15

5.5 Laser safety considerations

Before taking measurements in healthy volunteers, laser safety considerations of the whole AO-SLO-LSLO system have to be taken into account. In addition the measurements have to be approved by the local ethics committee. The

following laser power contributions were included into the considerations: [1].

1. The AO-SLO is operated at a central wavelength of 840nm. Due to scanning over an angle range of 1° with 4kHz line-scan rate and 20-40Hz frame rate in the x- and y-directions respectively, the allowed maximum power emission (MPE) yields 1.39mW according to laser safety standards.

2. The LSLO operates at a central wavelength of 1050nm. The total power is not focused on a single location on the retina but distributed over a whole line with an angle range of 14.1° (see 5.4). Hence, the MPE can be calculated for line illumination (from EN 60825-1) [26]:

$$MPE = 18\ C_7\ C_6\ C_4\ T_2^{-0.25} = 1283\ Wm^{-2} \tag{5.8}$$

where the parameters are $C_4 = 5,\ C_6 = \frac{\alpha}{\alpha_{min}} = 33.8,\ C_7 = 1$ and $T_2 = 10 \times 10^{(\alpha-\alpha_{min})/98.5} = 3.16s$ for the LSLO's wavelength range. Here, α is the angular subtense that must be set for values $\alpha > \alpha_{max} = 100mrad$:

$$\alpha = \frac{\alpha_{max} + \alpha_{max}}{2} = 50.75° \tag{5.9}$$

with $\alpha_{min} = 1.5°$ [26].

This yields a power of 49mW that can be applied to the eye. Having these aspects in mind, we need to ensure that the sum of the quotients (power/MPE) value is below 1:

$$\frac{P_{840}}{MPE_{840}} + \frac{P_{1050}}{MPE_{1050}} < 1 \tag{5.10}$$

Using the given power value of $P_{840} = 0.7$ for the AO-SLO, we can calculate a maximum power for the 1050nm light source with $P_{1050} = 8.1mW$. Measurements were performed on healthy volunteers with an incident power below 1.1mW which is way below the maximum power that is allowed within the laser safety standards.

5.6 Imaging Settings

This part describes the different settings of the camera and the scanner that were used in this thesis.

[1] This paragraph is adapted from the laser safety protocol of the Medical University of Vienna (see [32])

5.6.1 Camera settings

These settings can be changed using the program CameraControl.vi. The digital gain was set to 1 for SNR measurements. For in vivo measurements the digital gain was set to 2. Measurements on the artificial eye were performed with different exposure times ranging from 44.3ms to 353.9ms For in-vivo imaging, two different exposure times 353.2μs and 125.0 μs were used only. At the same time, the highest sensitivity setting of the camera (450 [e-/counts]) was used.

5.6.2 Scanner settings

A change in the exposure time settings for the camera results in different 2D image acquisition times. Thus, the scanning speed of the GS has to be adapted. This can be done using the program ScannerControl.vi. Table 5.5 shows the possible exposure times and corresponding GS settings.

Table 5.5: Settings of the GS for different exposure times.

Exposure time [μs]	Scanner amplitude [a.u.]	Number of lines [a.u.]
353.9	2000	1400
125.2	2000	550

Chapter 6

Results

During this thesis numerous artificial eye and in-vivo measurements were performed with the LSLO. In this chapter, representing imaging results are shown. Post-processing of the images included the adjustment of brightness and contrast using the open source software imageJ and frame averaging.

6.1 Model eye measurements

Before testing the LSLO performance on human subjects, we performed measurements on a model eye in order to evaluate several LSLO parameters such as the field of view, contrast and overall image quality. The model eye consists of an achromatic lens(f=30mm. d=2.54mm) and a sheet of paper. Figure 6.1 shows AO-SLO and LSLO images of the model eye. From the LSLO image a SNR of 28.38dB was calculated using digital gain of 2. Note that the AO-SLO image is greatly saturated when the AO-correction is turned on. One remaining problem of the setup is that AO-SLO images and LSLO images can not be recorded simultaneously. This would require the implementation of both data acquisition program into a combined program.

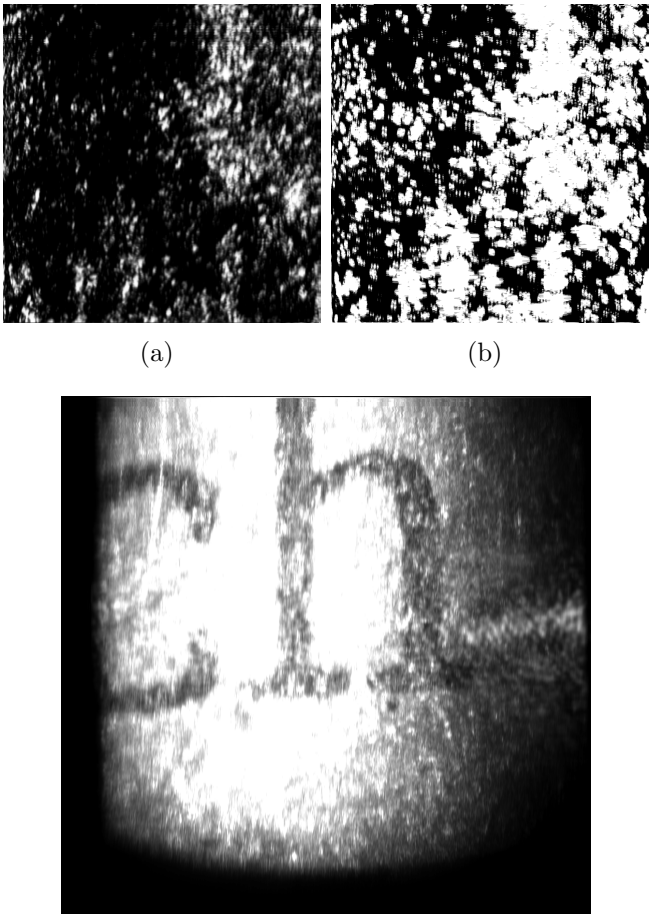

(a) (b)

(c)

Figure 6.1: Measurements of the the model using the AO-SLO without AO (a) and with AO correction (b) and a subsequent LSLO measurements (c) including the same model eye region at an exposure time of 125.0ms. AO images were averaged over 50 single frames, the LSLO image over 23 single frames.

6.2 In vivo measurements

Prior to imaging, informed consent was obtained and possible risks of the measurement have been explained. The study was performed under a protocol that had been approved by the local ethics committee of the Medical University of Vienna and which adhered to the tenets of the Declaration of Helsinki. Figure 6.2 shows an overview fundus image of a healthy eye taken with a commercial fundus camera (Spectralis, Heidelberg Engineering). The same eye was imaged with the LSLO and the imaging locations are marked with rectangles in the image.

Due to sensitivity issues of the used SHS, only LSLO images were recorded in vivo. Although AO-SLO images can be recorded with the system, the AO correction currently is quite unstable for in vivo applications. This prevented a simultaneous data acquisition using both the AO-SLO and the LSLO. Therefore only LSLO images are presented.

Figure 6.3 shows exemplary LSLO images at different locations of the retina. When comparing these images with the corresponding fundus image of the same eye in figure 6.2, we can easily determine the exact location of each individual image. In all images retinal vessels can be clearly identified.

Figure 6.4 shows an exemplary LSLO image of the nerve head region of a healthy volunteer. Main veins and arteries running to the nerve head are clearly visible. Figure 6.5 depicts the retinal profile along the yellow bar.

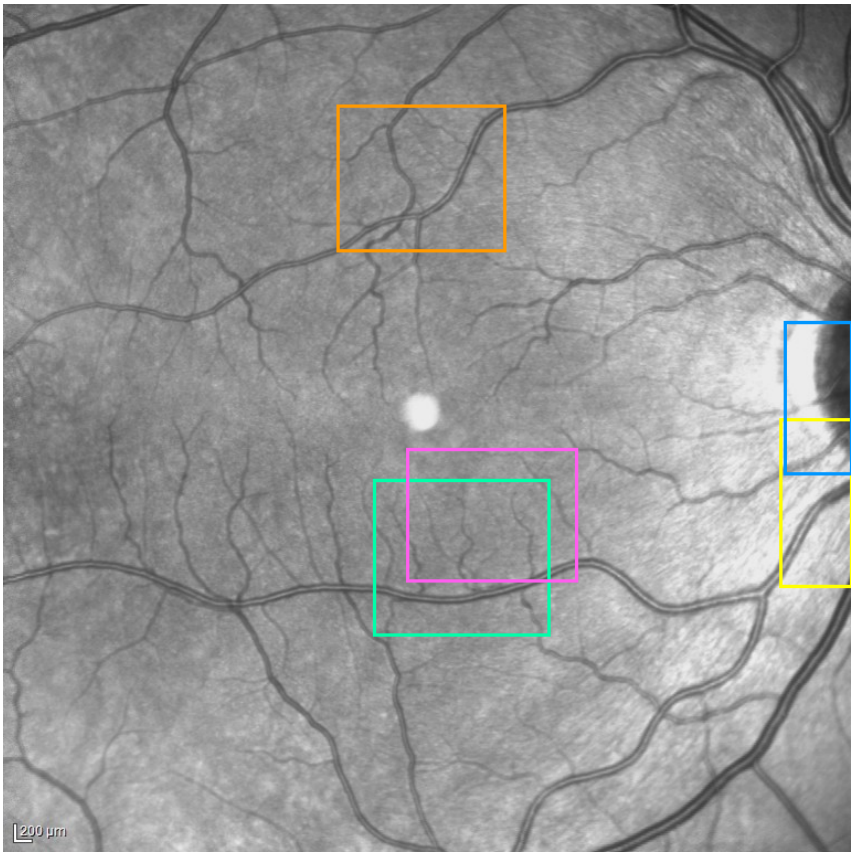

Figure 6.2: Fundus image of a healthy eye recorded with a commercial instrument. The coloured areas correspond each to the location of the LSLO images displayed in fig. 6.3, the yellow to figure (a), blue to fig. (b), orange to fig. (c),turquoise to fig. (4) ,and pink to fig. (e). The bright spot in the center of the image is an artifact caused by the corneal reflex).

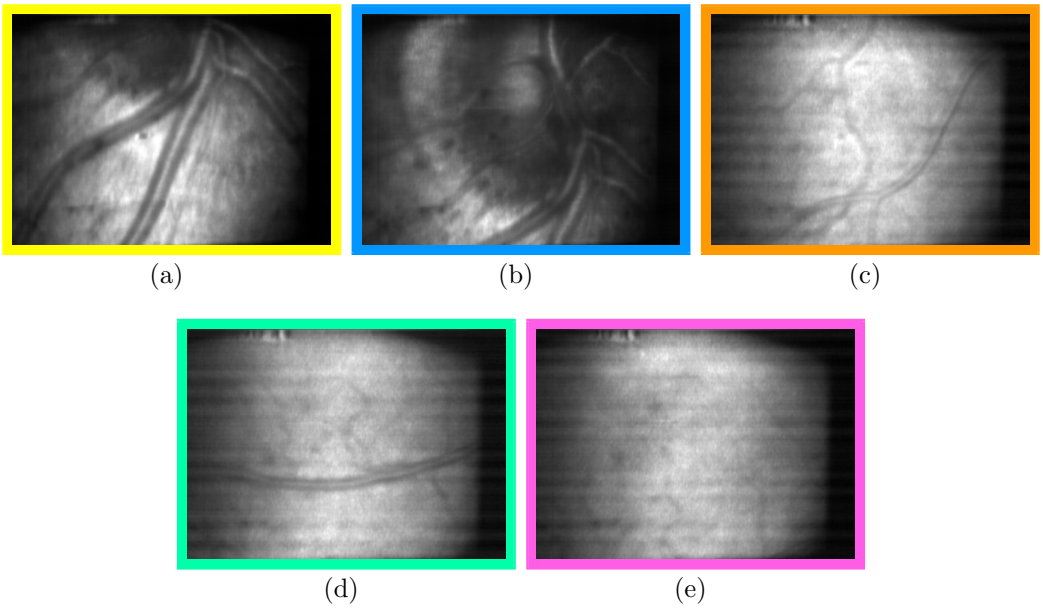

Figure 6.3: Exemplary LSLO measurements of a healthy volunteer. Exact location of each figure is shown in figure 6.2. Each image has a field of view of $7.2° \times 5.2°$.

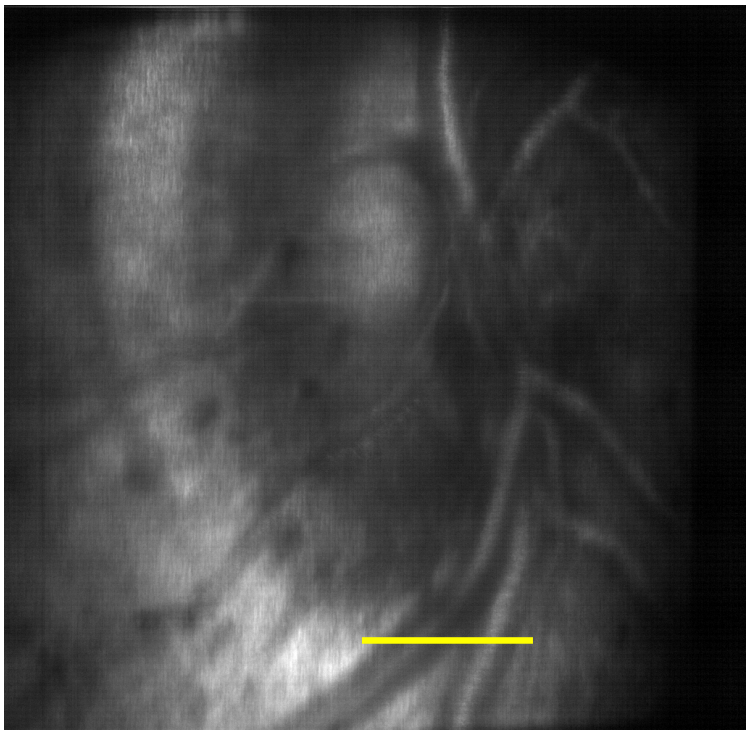

Figure 6.4: Exemplary single frame LSLO image of the nerve head of a healthy eye. The image size is 1024px and 1000px in the x- and y directions respectively. This corresponds to 4.02mm and 2.94mm respectively on the retina. (Assuming an eye-length of $\sim$ 22.5mm). The yellow line indicates the location of the intensity profile shown in figure 6.5

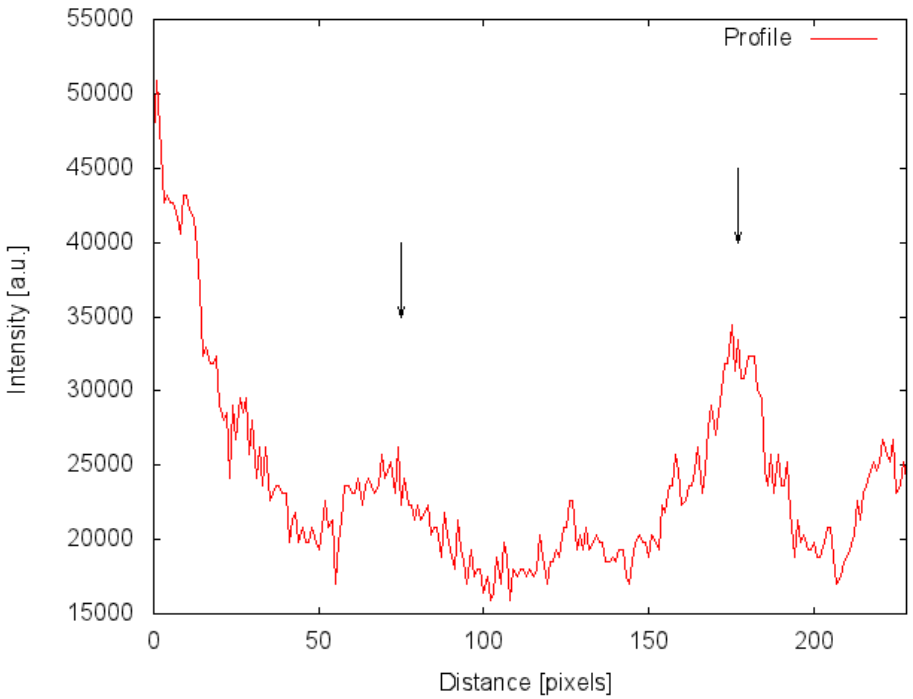

Figure 6.5: Line profile of the vessels in figure 6.4 marked with the yellow line. Arrows indicate the position of the blood vessels.

Chapter 7

Discussion and outlook

Within this thesis, a Line-Scanning Laser Ophthalmoscope was designed and implemented into an Adaptive Optics system. The LSLO's main goal is to provide larger field of view retinal images than what can be obtained with the AO-SLO. This enables to better locate the recorded high resolution, but small field of view images of the AO-SLO. The first chapter of this master thesis described different retinal imaging techniques and elaborated on advantages of LSLO. In the next chapter the AO-SLO system and the LSLO target design are introduced. In the following chapters, details of the LSLO imaging system and the alignment process are presented. Furthermore, an explanation of the system control software is given, finally the thesis describes the system's main characteristics and shows imaging results for the model eye and and in vivo in healthy volunteers.

The LSLO's main assets are the simple design and the straightforward implementation into the AO-SLO system. It produces larger field of view retinal images that simplify the determination of the imaging location of the AO-SLO system. The image quality provided by the LSLO is sufficient to even determine the imaging location of the AO-SLO online. Therefore patient alignment should be significantly improved. The final goal would be that LSLO and AO-SLO images are recorded simultaneously. This will simplify the comparison with other imaging modalities.

Currently, the simultaneous recording of both imaging modalities was not implemented. In order to achieve this goal the data acquisition software has to be adapted which could unfortunately not be achieved within the time frame of this thesis. In addition the SNR and finally the image quality may further be improved by increasing the power of the 1050nm beam. According to the

laser safety standards, a power of up to 8.1mW can be applied in addition to the AO-SLO illumination power which results in $\sim$ 9dB improvement of sensitivity. However, initial experiments with higher power (by removing the neutral density filter in front of the EC) showed that backreflections from lenses saturate the camera and prevent in-vivo imaging. Therefore the lower power was used within this thesis. In order to benefit from the higher power the problem of backreflections has to be solved.

One remaining problem of the setup is the cut off of the imaging beam by the used prisms. The implementation of larger prisms would increase the field of view not only in horizontal (x-) but also in vertical (y)-direction. Nevertheless, the current field of view is more than sufficient to determine the exact location of the LSLO image. The next important step requires the implementation of a simultaneous AO-SLO and LSLO data acquisition. After this is accomplished the AO correction performance needs to be tested. The beam propagation of the AO-SLO remained the same, however the DiM was inserted into the beam in order to combine both imaging beams. The influence of this DiM on the AO correction still needs to be determined. Finally the stability of the AO correction for in vivo measurements has to be improved.

The combined AO-SLO-LSLO system represents a powerful imaging modality that may be applied for patient imaging in near future. Since it is not possible to image the entire retina with the high-resolution provided by AO-SLO it is extremely important to focus only at regions of interest. Of specific interest are the margins of retinal lesions where both diseased and healthy tissue is present. With the online view provided by the LSLO the regions of interest can be much simpler found and the AO-SLO will provide the corresponding high resolution images of this region. These detailed images might allow better characterization of the disease and may provide a unique opportunity to monitor disease related changes of the retina on a cellular level.

Bibliography

[1] S. Resnikoff, D. Pascolini, D. Etyaale, I. Kocur, R. Pararajasegaram, G.P. Pokharel, S.P. Mariotti: *Bulletin of the World Health Organization* 82 (11), pp. 844-851, 2004

[2] F. Grehn, *Augenheilkunde*, Springer Medizin Verlag, 2007

[3] R.H. Webb, G.W. Hughes: *Scanning laser ophthalmoscope*, IEEE Transactions on Biomedical Engineering 28 (7), pp. 488-492, 1981

[4] D.R. Williams: *Imaging single cells in the living retina*, Vision Research 51, pp. 1379-1396, 2011

[5] A. Roorda, D.R. Williams: *The arrangement of the three cone classes in the living human eye*, Nature 397 (6719), pp. 520-522, 1999

[6] W. Krebs, I. Krebs: *Primate retina and choroid: atlas of fine structure in man and monkey*, Springer-Verlag New York Inc., 1991

[7] J. Porter, H. Queener, J. Lin, K. Thorn, A. Awwal: *Adaptive Optics for Vision Science*, John Wiley & Sons, Inc., 2006

[8] A. Dubra, Y. Sulai, J.L. Norris, R.F. Cooper, A.M. Dubis, D.R. Williams, J. Carroll: *Noninvasive imaging of the human rod photoreceptor mosaic using a confocal adaptive optics scanning ophthalmoscope*, Biomedical Optics Express 2 (7), pp. 1864-1876, 2011

[9] D.X. Hammer, R.D. Ferguson, T.E. Ustun, C.E. Bigelow, N.V. Iftimia, R.H. Webb: *Line-scanning laser ophthalmoscope*, Journal of Biomedical Optics 11 (4), art. no. 041126, 2006

[10] P.F. Sharp, A. Manivannan, H. Xu, J.V. Forrester *The scanning laser ophthalmoscope - a review of its role in bioscience and medicine*, Physics in Medicine and Biology 49, pp. 1085-1096, 2004

[11] R.H. Webb, G.W. Hughes, F.C. Delori: *Confocal scanning laser ophthalmoscope*, Applied Optics 26 (8), pp. 1492-1499, 1987

[12] D. Huang, E.A. Swanson, C.P. Lin, J.S Schuman, W.G. Stinson, W. Chang, M.R. Hee, (...), J.G. Fujimoto: *Optical Coherence Tomography*, Science 254 (5035), pp. 1178-1181, 1991

[13] M.E.J. van Velthoven, D.J. Faber, Frank D. Verbraak,T.G. van Leeuwen, M.D. de Smet: *Recent developments in optical coherence tomography for imaging the retina*, Progress in Retinal and Eye Research 26 (1), pp. 57-77, 2007

[14] A.F. Fercher, W. Drexler, C.K. Hitzenberger, T. Lasser: *Optical coherence tomography - principles and applications*, Reports on progress in physics (66), pp. 239-303, 2003

[15] M. Pircher, R.J. Zawadzki: *Combining adaptive optics with optical coherence tomography: unveiling the cellular structure of the human retina in vivo*, Expert Review of Ophthalmology 2 (6), pp. 1019-1035, 2007

[16] M. Lombardo, S. Serrao, N. Devaney, M. Parravano, G. Lombardo *Adaptive Optics Technology for High-Resolution Retinal Imaging*, Sensors 2013, 13(1), pp. 334-366, 2013

[17] A. Roorda: *Applications of Adaptive Optics Scanning Laser Ophthalmoscopy*, Optom. Vis. Sci. 87 (4), pp. 260-268, 2010

[18] A. Roorda: *Adaptive optics for studying visual function: A comprehensive review*, Journal of Vision 11(5):6, pp. 1-21, 2011

[19] P. Godara, A.M. Dubis, A. Roorda, J.L. Duncan, J. Carroll: *Adaptive Optics Retinal Imaging: Emerging Clinical Applications*, Optometry and Vision Science 87 (12), pp. 930-941, 2010

[20] A. Dubra, Y. Sulai: *Reflective afocal broadband adaptive optics scanning ophthalmoscope*, Biomedical Optics Express 2 (6), pp. 1757-1768, 2011

[21] F. Felberer, J. Kroisamer, C.K. Hitzenberger, M. Pircher: *Lens based adaptive optics scanning laser ophthalmoscope*, Optics Express 20 (16), pp. 17297-17310, 2012

[22] D. Scoles, Y.N. Sulai, A. Dubra: *In vivo dark-field imaging of the retinal pigment epithelium cell mosaic* D. Scoles, Y.N. Sulai, A. Dubra, Biomedical Optics Express 4 (9), pp. 1710-1723, 2013

[23] J. Carroll, D.B. Kay, D. Scoles, A. Dubra, M. Lombardo: *Adaptive Optics Retinal Imaging - Clinical Opportunities and Challenges*, Current Eye Research 38 (7), pp. 709-721, 2013

[24] G.Aschinger: *Master thesis, Adaptive Optics Scanning Laser Ophthalmoscope*, 2012

[25] NP Photonics: *Scorpion 1-um ASE Module Operating Instructions & User Manual, Version 1.8*, 2005

[26] International Electrotechnical Commission: *IEC 60825-1 International standard - safety of laser products*, Edition 1.2, 2001

[27] Thorlabs Inc.: *http://www.thorlabs.de/catalogpages/V21/978.PDF*, 28/08/2013

[28] SUI, Goodrich Corporation: *Operation Manual: LDH2, 92kHz InGaAs Linescan Camera for OCT*, 2010-2011

[29] W. Demtröder: *Experimentalphysik 2, Elektrizität und Optik*, Springer, 2006

[30] OZ Optics Ltd.: *http://www.ozoptics.com/ALLNEW_PDF/DTS0079.pdf*, 2/12/2013

[31] OZ Optics Ltd.: *http://www.ozoptics.com/ALLNEW_PDF/DTS0094.pdf*, 2/12/2013

[32] M. Pircher: *Untersuchung von zellulären Strukturen der Netzhaut mittels adaptiver Optik unterstützten OCT/SLO an gesunden Probanden und Patienten mit Nezthautveränderungen - eine Pilotstudie EK Nr. 1437/2013*, 2013

List of Figures:

http://www.thorlabs.de/images/TabImages/DMSP1000_Unpolarized_780px.gif, 21/08/2013